Novel liquid crystal photonic devices enabled by two-photon polymerization [invited]

ZIQIAN HE,[1] GUANJUN TAN,[1] DEBASHIS CHANDA,[1,2,3,4] AND SHIN-TSON WU[1,*]

[1]*College of Optics and Photonics, University of Central Florida, Orlando, FL 32816, USA*
[2]*Department of Physics, University of Central Florida, Orlando, FL 32816, USA*
[3]*NanoScience Technology Center, University of Central Florida, Orlando, FL 32826, USA*
[4]*Debashis.Chanda@creol.ucf.edu*
swu@creol.ucf.edu

Abstract: In addition to displays, liquid crystals (LCs) have also found widespread applications in photonic devices, such as adaptive lens, adaptive optics, and sensors, because of their responses to electric field, temperature, and light. As the fabrication technique advances, more sophisticated devices can be designed and created. In this review, we report recent advances of two-photon polymerization-based direct-laser writing enabled LC devices. Firstly, we describe the basic working principle of two-photon polymerization. With this powerful fabrication technique, we can generate anchoring energy by surface morphology to align LC directors on different form factors. To prove this concept, we demonstrate LC alignment on planar, curvilinear surfaces as well as in three-dimensional volumes. Based on the results, we further propose a novel, ultra-broadband, twisted-nematic diffractive waveplate that can potentially be fulfilled by this technique. Next, we briefly discuss the current status of direct-laser writing on LC reactive mesogens and its potential applications. Finally, we present two design challenges: fabrication yield and polymer relaxation/deformation, remaining to be overcome.

1. Introduction

Liquid crystals (LCs) are self-assembled soft materials composed of certain anisotropic molecules with orientational orders. They respond to external stimulus such as heat, electric field, magnetic field, and light [1–6]. In the presence of an electric field, these anisotropic organic compounds with both optical and dielectric anisotropies can be reoriented, resulting in intensity and/or phase modulation. Nowadays, liquid crystal displays (LCDs) have become ubiquitous in our daily lives [7,8]; their applications span from smartphones, pads, computer screens, to large-sized TVs. In addition to displays, LC devices have also found useful applications in beam steering [9–11], optical communications [12–14], lighting applications [15–17], smart windows [18–20], tunable metasurfaces [21–23], and augmented reality and virtual reality systems [24–26], just to name a few. To manipulate electro-optical properties and thus accomplish different device functions, strategies including special electrode designs, compound structures, and spatially variant alignment can be utilized. Among them, spatially variant alignment has attracted a lot of attentions. After the advent of photoalignment materials where complicated LC arrangement can be easily achieved by patterning the photosensitive layer with a spatially variant linearly polarized light [27–29]. As the alignment technique evolves, we foresee novel and even more sophisticated LC devices to be demonstrated in the near future. On the other hand, LC elastomers or networks have also attracted extensive attention in fundamental researches. Generally, LC elastomers or networks are low-density crosslinked LC mixtures. These special materials combine the properties of polymeric elastomers with LCs [30–33]. They are promising as soft actuators and sensors in that their shape can be reversibly adjusted according to the external stimulus [34–36]. The

mechanical motion upon external stimulus is related to the alignment and phase transition of the employed LC. Depending on the alignment and mixture materials, contraction, bending, or rotation can be observed [37–39]. Thus, LC elastomers are promising candidates for soft robotics, smart micro/nanostructures, and tunable photonic devices [40–42].

In recent years, the development of ultrafast laser systems has enabled novel applications in material processing based on nonlinear light-matter interactions [43,44]. An intriguing bottom-up three-dimensional (3D) micro- and nano-fabrication technique based on high-intensity laser pulses is the two-photon polymerization (TPP) of photosensitive materials [45–48]. In a typical TPP process, high-intensity laser pulses inaugurate the crosslinking of photoresist via two-photon absorption within a localized focal volume, i.e. a voxel. This property differentiates TPP from the traditional photolithography and results in ultrafine 3D micro- and nano-structures. To date, TPP-based direct laser writing (DLW) has given rise to an abundance of researches on fabrication of optical components, photonic and acoustic structures, and biocompatible materials and structures [49–52].

In this paper, we briefly review recent advances on TPP-enabled fabrication techniques and then focus on some new TPP-assisted LC photonic devices. In Section 2, we introduce the working principle of TPP. In Section 3, we illustrate how to use TPP to generate desired LC alignment layer in two-dimensional (2D) surfaces, curvilinear surfaces (2.5D), and 3D volumes. Based on the potential of using TPP to generate 3D scaffold, we further propose a broadband diffractive waveplate for beam steering and theoretically evaluate its performance. In Section 4, we briefly discuss the use of TPP to directly write on LC reactive mesogens and its applications. Finally, in Section 5, we highlight two technical challenges of using TPP for novel LC devices: fabrication yield and photoresist relaxation.

2. Two-photon polymerization direct-laser writing

Figure 1 illustrates the working principles of traditional photolithography and TPP process. The former utilizes single-photon absorption (usually UV light) of photoresist to create arbitrary 2D pattern or holographic 3D pattern by multi-beam interference, while the latter uses two-photon absorption, which requires a much higher intensity of the laser beam (usually at near infrared wavelength) [53]. Because of the high laser-intensity threshold and nonlinear nature of the process, a resolution beyond the diffraction limit can be realized by controlling the laser pulse energy. Previous reports have successfully predicted the size of the polymerized volume (volume pixel or voxel) by defining a polymerization threshold. As a result, voxel size as small as ~100 nm can be generated and therefore this technique provides much better structural resolution and quality than the traditional stereolithography method [48].
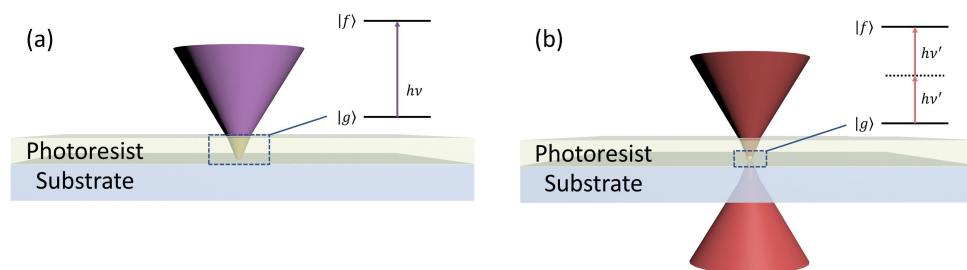

Fig. 1. Working principles of (a) traditional UV photolithography and (b) TPP. The dashed rectangles highlight the polymerized volume. In traditional photolithography, almost all the exposed volume is polymerized due to the low threshold of single-photon absorption. While for TPP, only a localized focal volume is polymerized.

In general, as Fig. 2 depicts, there are three working configurations of TPP: air mode, oil-immersion mode, and dip-in mode. In air mode, there is an air gap between photoresist and

objective lens, and the substrate is inverted in *z*-axis (facing down). In oil-immersion mode, the substrate is upward and immersion oil is applied between the substrate and the objective to reduce refraction-related aberrations. In dip-in mode, the substrate is inverted in *z*-axis and the objective is directly immersed into the photoresist. Among these three modes, dip-in mode provides the highest resolution (least aberration), and comparing to oil-immersion mode it offers a larger maximum feature height. To arbitrarily and accurately pattern 3D features, a laser scanning system is applied with computer-controlled positioning systems. Here we use a commercialized laser lithography system (NanoScribe GmbH) to perform TPP processing, with a 780-nm pulsed laser and dip-in mode is applied. Highly accurate positioning systems including piezoelectric stage (for *x*, *y*, and *z* axes) for moving samples and galvanometer scanner (for *x* and *y* axes) for steering laser beams are employed to fully benefit from the inherent high-resolution of TPP process. To specify, piezoelectric stage can travel at the range of centimeter while it needs time to stabilize and the moving speed is limited. On the other hand, galvanometer scanner offers faster scanning in the writing plane but with limited travel range (~100 μm). Thus, when writing a relatively large pattern, the strategy is to divide the pattern into several areas, followed by moving the writing area using piezoelectric stage and finishing writing in each area using the galvanometer scanner.
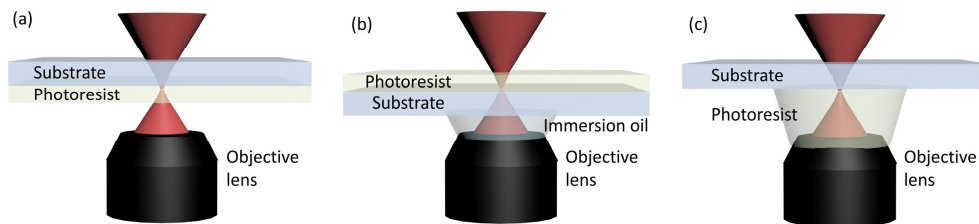

Fig. 2. Three working configurations of TPP: (a) air mode, (b) oil-immersion mode, and (c) dip-in mode. Among them, dip-in mode suffers from least aberration and thus offers highest resolution.

Due to the extraordinary ability of generating high resolution 3D patterns, a plethora of studies have used this technique to fulfill various demands. Moreover, as the TPP technique is still advancing [54–56], more original and inspiring researches can be expected.

3. Two-photon polymerization for liquid-crystal alignment

Previously, TPP has been applied to form micro surface-relief gratings (or microgrooves) [57] which offers anchoring energy to LCs. For a typical surface morphology-induced anchoring, a smaller grating period results in larger anchoring energy (10^{-5}~10^{-6} J/m^2 depending on the employed materials and grating periods) and many have demonstrated the potential of this technique in uniform or simple space-variant LC alignment [58–61]. Next, we delve into this discussion with emphasis from the device viewpoint.

3.1 Planar surface (2D) alignment

Currently, most of the studies are focused on planar surface alignment as this is the simplest case yet it is fundamentally important. Here, we begin our discussion with the basic binary LC gratings enabled by surface alignment. These binary gratings are especially useful for optical switches, beam steering, and advanced LCDs [62,63]. Pioneering works have achieved these devices through periodically patterning LC alignment by mechanical rubbing [64,65] or photoalignment techniques [66–69]. The main feature of these devices is the alternatively changing alignment directions on one substrate (these devices usually consist of two substrates), as depicted in Fig. 3. The green lines in Fig. 3 show the alignment direction and the yellow ellipsoid exhibit LC directors near the alignment surface. By arranging different alignment directions in space, 1D (Fig. 3(a)) and 2D (Fig. 3(b)) binary LC gratings

can be achieved no matter whether the other substrate is uniform alignment or patterned alignment.
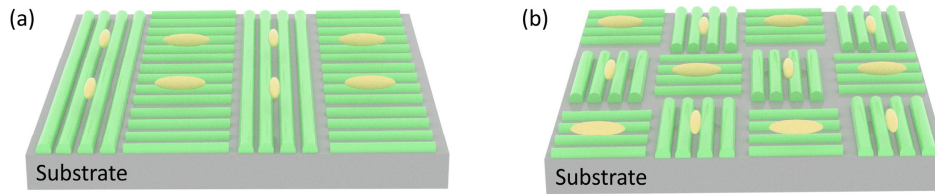

Fig. 3. The main feature of (a) 1D and (b) 2D binary LC gratings on one substrate. The green lines denote the direction of microgroove alignment and the yellow ellipsoids show the LC directors near the alignment surface.
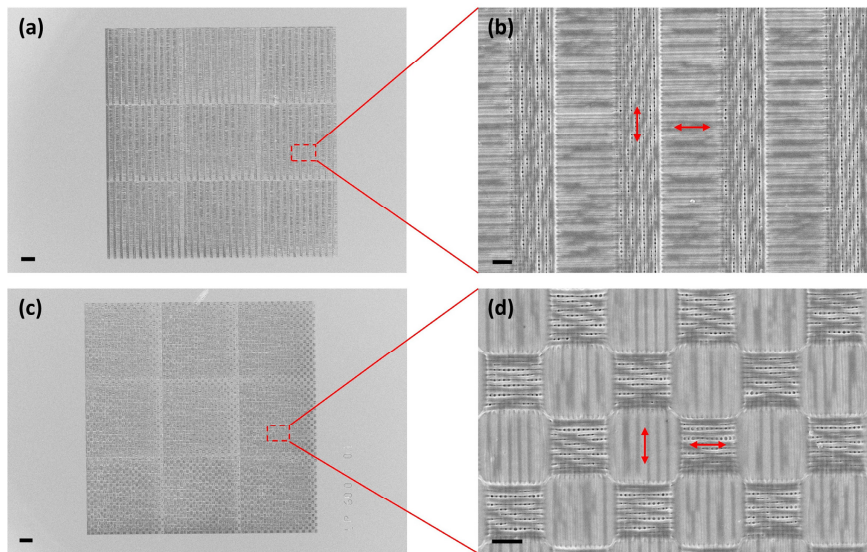

Fig. 4. SEM images of (a, b) 1D and (c, d) 2D grating alignment on one substrate where the nanogrooves have 300-nm period and the red arrows highlight the local LC alignment directions. Scale bar: 20 μm (a), 2 μm (b), 20 μm (c), and 2 μm (d).

As an alternative, TPP is also capable of producing such surface alignment. Micro-grating alignment with a block size of 10s microns has been demonstrated in 2015 [60]. Here, we apply the laser-writing system to show an even finer grating feature. The scanning electron microscopy (SEM) images are shown in Fig. 4. During the exposure, the high-power laser scans at the substrate-photoresist interface in a line-by-line fashion, resulting in nanogrooves with 300-nm line period and 100-nm depth. The period of the final 1D grating (Figs. 4(a) and 4(b)) is 7.2 μm while that of the 2D grating (Figs. 4(c) and 4(d)) is 7.2 μm in both orthogonal directions. We have further tested the alignment by assembling a LC cell where uniformly rubbed alignment, parallel to one of the patterned alignment directions, is formed on the other substrate. The LC cell gap (d) and material fulfil the first minimum condition of 90° twisted-nematic (TN) mode as [70]:

$$d\Delta n = (\sqrt{3}/2)\lambda, \tag{1}$$

where Δn is the birefringence of the LC and λ is the operating wavelength. It is turned out that such gratings with 7.2-μm grating period can be aligned well.

After examining the simplest alignment patterns, we can further target on more complicated cases. Our group has recently demonstrated the potential of arbitrary 2D LC alignment pattering by assembling single-side aligned LC microlens arrays based on Pancharatnam-Berry (PB) phase (or geometric phase) [71]. Unlike the traditional dynamic phase introduced via optical path difference, PB phase corresponds to the phase shift induced by the changes in other light wave parameters [72,73]. A commonly employed method for generating LC-based PB phase elements is by patterning half-wave plates in a spatially variant manner. Denoting the optical axis as $\varphi(x, y)$ and ignoring the common phase term, a circularly polarized input light will change its handedness with an extra phase term (2φ) after passing through the half-wave plates. This can be described by Jones matrix as:

$$J_{\pm} = \frac{1}{\sqrt{2}}\begin{bmatrix} \cos 2\varphi & \sin 2\varphi \\ \sin 2\varphi & -\cos 2\varphi \end{bmatrix}\begin{bmatrix} 1 \\ \pm i \end{bmatrix} = \frac{1}{\sqrt{2}}\begin{bmatrix} 1 \\ \mp i \end{bmatrix}e^{\pm 2i\varphi}. \tag{2}$$

With this powerful tool, we are able to create desired phase distribution for a PB microlens array via alignment patterning. Figure 5(a) demonstrates the LC alignment pattern on one substrate with a highlight on the LC director distribution for an individual microlens, while the working principle of the PB microlens array is illustrated in Figs. 5(b) and 5(c). Note that other than assembling a cell, this device can also work as passive elements through spin-coating reactive mesogen with certain thickness (that fulfils half-wave condition) and then UV curing. For such a passive device or an active device at voltage-off state, if it serves as converging lenses for right-handed circularly polarized light (RCP), it will diverge left-handed circularly polarized light (RCP), or vice versa.
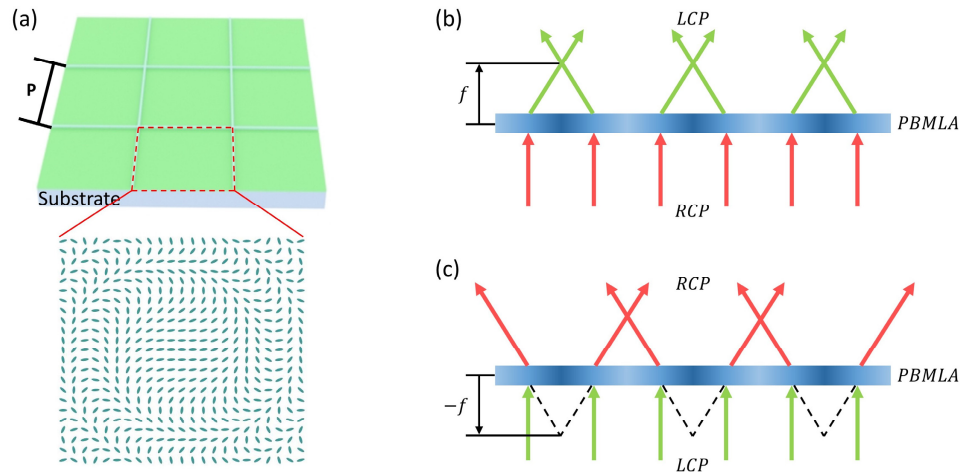

Fig. 5. (a) Schematic illustration of the patterned alignment layer on one substrate for a PBMLA. The highlight shows the desired LC alignment for a single microlens. In experiment, P = 148 μm. (b, c) Working principle of the PBMLA. When the PBMLA serves as converging lenses for RCP, it serves as diverging lenses for LCP. PBMLA: Pancharatnam-Berry microlens array.

An advantage of 2D nanogroove alignment is that it is compatible with nanoimprint lithography (NIL) [74–76]. NIL can boost the fabrication yield because of its relatively simple and quick processes. In experiment, a stamp was first cast from the master with nanogrooves (600-nm line period) made from TPP. Then, through NIL, the alignment pattern can be readily transferred onto a substrate coated with SU-8 photoresist. Figure 6 exhibits the SEM images of the imprinted pattern. The design of phase profile is in a discrete sense, as defined by different zones. In each zone, the alignment is uniformly oriented toward one

direction and there are at least five zones within 180° rotation of the alignment directions. The zone directions are defined to match the target LC director orientations. The directions of the nanogrooves can be clearly distinguished from one zone to another and if filled with LCs, the LC directors will be aligned along the nanogrooves. Some spaces were left blank to let LCs rotate freely between two different zones. It was also studied that the discrete nature of the phase introduced by the zones only slightly diminishes the efficiency and peak intensity. From the angled view (Fig. 6(d)), the 2D flat pattern can be observed. By further assembling a single-side aligned LC cell with 1.6-μm cell gap, it shows that the focal length of the microlens array is around $\pm$ 2.49 mm at 633 nm, $\pm$ 2.84 mm at 546 nm, and $\pm$ 3.40 mm at 450 nm. The corresponding efficiency at voltage-off state is 47.2% for 633 nm, 57.6% for 546 nm, and 52.2% for 450 nm (defined as the ratio of the optical power of focused beam to that of circularly polarized incident beam). The efficiency is not very high due to some misalignment especially at corners where the spatial frequency is the highest, and the diffraction effect of the array, digitized phased profile, etc. Nevertheless, such a microlens array exhibits good image quality at 8 V_{rms} with a switching time of 3.57 ms, which is much faster than a refractive microlens. The good quality ensures the feasibility of patterning arbitrary 2D alignment using TPP (and potentially combined with NIL). A variety of waveplates [77–84] should be attainable by this technique.
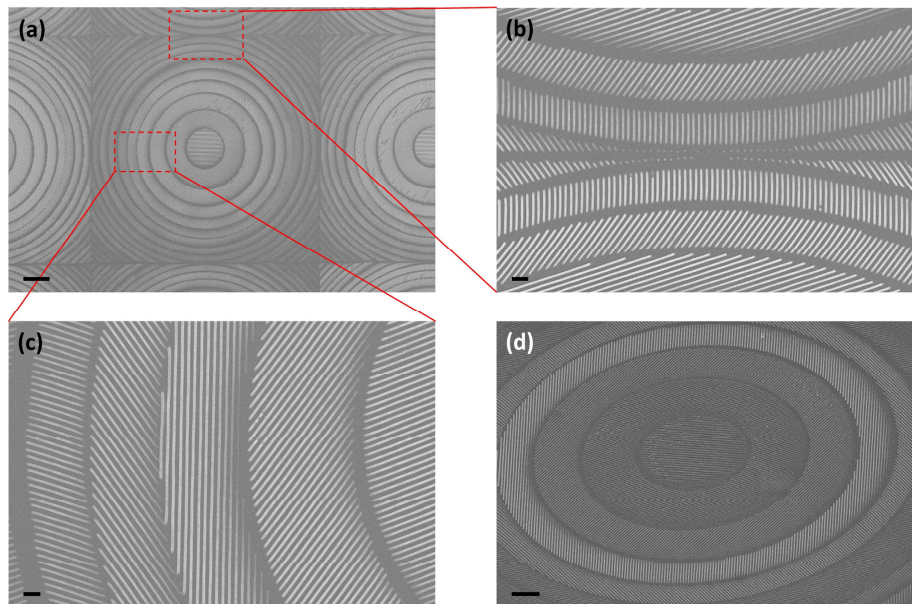

Fig. 6. SEM images of the imprinted alignment for a PB microlens array. (a) Top view where (b, c) are zoom-in views showing the nanogrooves orienting at different directions. (d) Angled view. Scale bar: 20 μm (a), 2 μm (b), 2 μm (c), and 10 μm (d).

Beside arbitrary 2D patterning, another interesting aspect is that degenerate alignment (or multi-stable alignment) can be fulfilled through this method. This kind of alignment is important for both fundamental studies and energy-saving devices [85,86]. A schematic plot is shown in Fig. 7. In an original work [87,88], 2D grids with 300-nm line period were formed by TPP and cast into a stamp. After the pattern was transferred onto a substrate and a thin aluminum film (30 nm) was subsequently deposited, another ITO-glass substrate with homogeneously rubbed alignment was adhered to it and a LC cell can be accomplished. This device exhibited tunable reflective color when different voltages were applied, which was explained by grating-coupled propagating surface plasmon modes. The patterned substrate consists of square lattices with lattice constant 300 nm, achieved by polymerizing lines in

both orthogonal directions in-plane. It was discovered that the LC director distribution should have degeneracy in both orthogonal directions. It can be expected that other kinds of degeneracy should be achievable through surface morphology engineering.
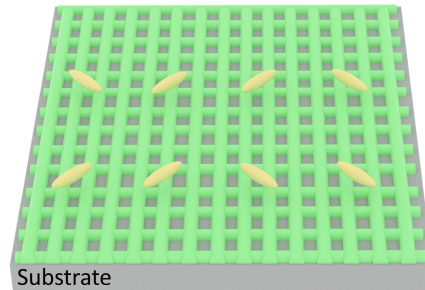

Fig. 7. Schematic plot of two-state degenerate alignment achieved by TPP. Polymerizing the lines (green grids) in both orthogonal directions in plane, the LC directors (yellow ellipsoids) are degenerate in both diagonal directions.

3.2 Curvilinear surface (2.5D) alignment

A prominent example of 2.5D alignment was demonstrated as a composite-lens type refractive LC microlens array. These tunable-focus liquid crystal (LC) microlens arrays are an essential optical component for image processing [89,90], beam steering [91,92], wavefront correction [93] and switchable 2D/3D displays [94]. Figure 8(a) illustrates the schematic plot of such a LC microlens array. It consists of a passive microlens array (can be polymer or others) and a uniform alignment layer on top of that. After the LC cell is finished, the LCs will be alignment along one direction, resembling homogeneous alignment. The working principle utilizes the dielectric constant difference between LCs and passive lenses as well as the birefringence of the LCs (Figs. 8(b) and 8(c)). If LCs and passive lenses have distinct dielectric constant, when applying appropriate voltages, the voltage shielded by the passive lenses will vary according to its thickness. This in turn results in different phase delay across the lens and thus leads to tunable focal lengths. An intrinsic property of this type of lenses is that they are bi-focal. The focal length is tunable only for one linear polarization of light that is parallel to the alignment direction.
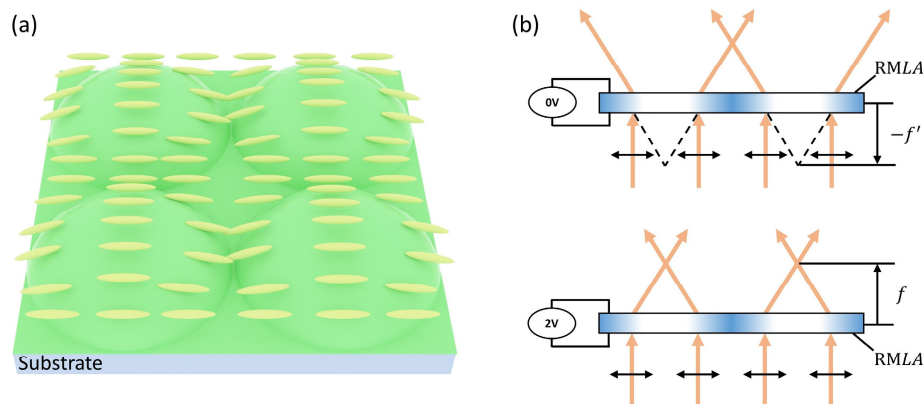

Fig. 8. (a) Schematic illustration of the composite-lens type LC microlens array. (b, c) An example showing the working principle of RMLA. As a bi-focal lens, the focal length is tunable only for one linear polarization of light (parallel to the alignment direction). By applying different voltages, the RMLA can either diverge or converge input light. RMLA: refractive microlens array.

Previously, to achieve a composite lens, the alignment and the passive lenses are created independently [95]. By TPP, the composite lens and alignment layer can be generated simultaneously [96]. Figure 9 demonstrates the slanted SEM images of fabricated polymer microlens with nanogroove alignment (700-nm line period). The size of each microlens is 120 $\times$120 μm^2 and the height is 5 μm. The nanogroove alignment can be clearly observed from the zoom-in view (Fig. 9(b)) where the red arrow highlights the alignment direction. This patterned substrate can then be adhered to another substrate with alignment parallel to the nanogroove direction and a LC test cell can be formed. It was revealed that the alignment on the passive microlenses shows polar pretilt-angle effect, which was not observed in planar structures. Further testing ensured its good focusing and image quality.
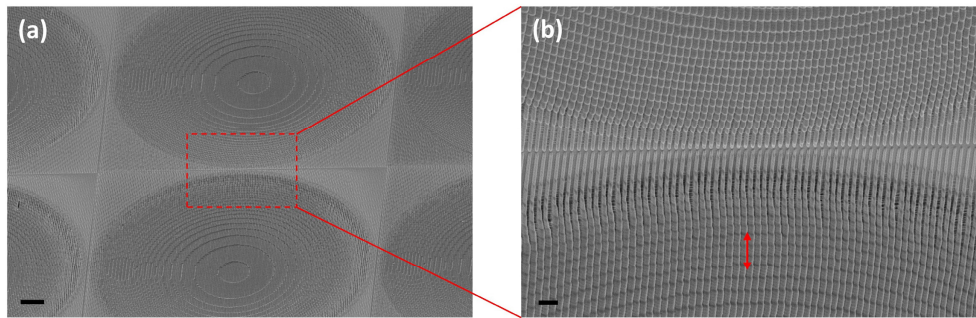

Fig. 9. Slanted SEM images of the passive refractive microlens array with nanogroove alignment fabricated by TPP. (a) Top view where (b) is a zoom-in view showing the nanogrooves orienting uniformly toward one direction as the red arrow denotes. Scale bar: 20 μm (a), 2 μm (b).

3.3 Bulk (3D) alignment

While photoalignment, rubbed alignment, and TPP-based alignment can all work for surfaces with good UV/heat stability, the latter exhibits unique potential to organize LC directors in bulk. Here, we initiate the discussion with the simplest case, which is organized multi-layer LC devices.

Figure 10 displays the configuration of three dual-layer LC devices. For phase modulators, the cell resembles homogeneous alignment except that an additional polymer layer with nanogroove alignment is inserted into the cell. For polarization-independent phase modulators, the LC alignment directions should be orthogonal in the two LC layers with equal thickness. The alignment of dual-layer TN resembles that of traditional TN and the inserted polymer layer offers alignment having 45° relative to the substrate alignment. The fabrication strategy of the 3D scaffold for all three devices are similar. Figure 11 demonstrates the strategy of fabricating 3D scaffold for the dual-layer TN in detail.
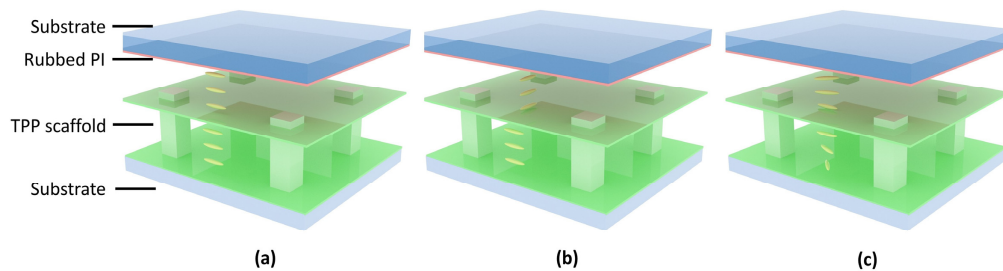

Fig. 10. Schematic illustration of three dual-layer LC devices: (a) phase modulator, (b) polarization-independent phase modulator and (c) TN. The green structures are 3D scaffolds fabricated by TPP and the yellow ellipsoids are LC directors.
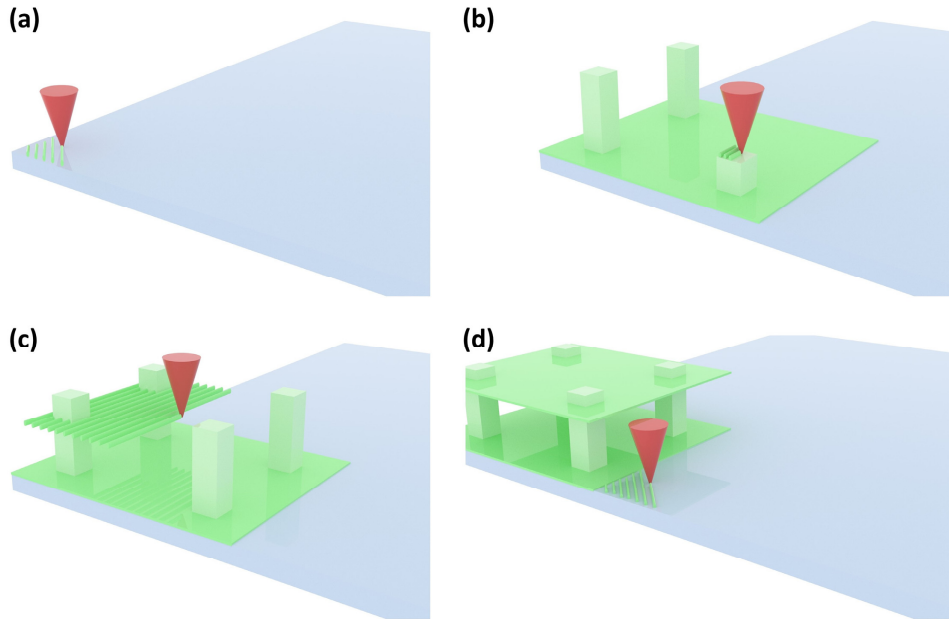
Fig. 11. Step-by-step fabrication process of the 3D scaffold for dual-layer TN. After dropping photoresist on the substrate, a laser lithography system is applied to expose the photoresist line-by-line. During the exposure, the entire structure will be divided into many writing fields, determined by the objective and the laser scanning system. The polymerization process happens at one writing field at a time. (a) Line-by-line exposure to form a uniform groove alignment covering one writing field. (b) After the bottom alignment layer is exposed, the laser will then polymerize pillars that are used to support the floating layer. (c) Line-by-line exposure to form the floating layer which offers alignment at 45° relative to the bottom alignment. (d) After finishing this writing field, the laser system will move to the next writing field and keep scanning until the whole structure is accomplished.

The major advantage of multi-layer phase modulator is that one can engineer the response time and driving voltage in a controllable way, compared with polymer-network LC (PNLC) [97]. In multi-layer phase modulators, the total phase change (δ) is governed by LC birefringence (Δn), total LC thickness (d) and wavelength (λ) as:

$$\delta = 2\pi d \Delta n / \lambda. \tag{3}$$

Meanwhile, the response time (τ) of the LC device is determined by:

$$\tau = \gamma_1 d_s^2 / (K\pi^2), \tag{4}$$

where γ_1 is the rotational viscosity, K (K_{11} is applied in homogeneous mode) the elastic coefficient of the employed LC and d_s the thickness of thickest LC sub-layer. In experiment, the response time improvement of dual-layer and three-layer phase modulators in reference to traditional phase modulators were 4 and 7 times faster, respectively. On the other hand, the driving voltage of such multi-layer devices increases linearly as the number of LC layers increases. Other advantages of multi-layer phase modulators comparing to PNLC are the reduced scattering and diminished hysteresis [97].

Regarding to polarization independent phase modulators, the previous approaches either requires high operation voltage [98,99], or can hardly achieve 2π phase change [100], or show limited reliability [101]. By multi-layer approach, all abovementioned challenges can be solved [102]. In experiment, a relatively large area sample (3.3×3.3 mm^2) with 91% aperture ratio was fabricated. Through Mach-Zehnder interferometer testing, such a device exhibited

good polarization independency with ~10 V_{rms} full-operation voltage (2π phase change at 633 nm) and 8.85-ms relaxation time (100% to 10%).

To benefit from this general strategy of boosting LC device response time, dual-layer TN samples are fabricated, and the performance is further investigated here. Specifically, to fabricate the polymer scaffold, dip-in mode was used with a ×63, 1.4 numerical aperture (NA) objective (Zeiss) and IP-Dip (Nanoscribe GmbH) photoresist. The TPP process followed the strategy shown in Fig. 11 with line period of 300 nm. After the main structure was finished, there were some polymer spacers (pillar-shape) formed in the peripheral region to help maintain an appropriate cell gap in the functional area (useful for later assembling the LC cell). Then, the sample was gently immersed into 1,2-Propanediol monomethyl ether acetate (PGMEA) solution for 20 min to remove the unexposed photoresist, and subsequently it was placed in isopropyl alcohol (IPA) for 5 min to remove PGMEA. Last, to evaporate the IPA, the sample was held at 20 cm above a 200 °C hot plate until all the droplets were completely evaporated. To assemble the LC cell, a single-side ITO-coated glass substrate with alignment perpendicular to that of the bottom alignment was adhered to the structured substrate using NOA 81. Once UV cured, the test cell was filled with a LC mixture ZLI 4389 (Merck) under 10 Torr environments. This LC material has appropriate birefringence for TN at visible wavelength ($\Delta n = 0.16$ at $\lambda = 632.8$ nm, $\Delta\varepsilon = 45.6$ at 1 kHz driving frequency). For a fair comparison, the control single-layer TN device kept the same total effective LC-layer thickness and was filled with the same LC materials.

Figure 12 demonstrates the electro-optical properties of both dual-layer TN and control device. When measuring time-intensity and voltage-intensity responses, the devices were inserted in between two cross polarizers and the polarizers were aligned such that the devices showed maximum transmittance at voltage-off state. From the measurements, the dual-layer sample demonstrates 3.6 times improvement on response time (relaxation time) comparing to the control device. However, due to the extra alignment layer in the cell, the dual-layer sample exhibits a larger turn-on voltage due to the voltage shielding of the polymer layer, and some residue phases because of the extra alignment. It also worth mentioning that the bright and dark states of the dual-layer sample is somewhat degraded comparing to the control device. This can be ascribed to the polymer pillars (to support the floating layer) as they are not functional and can scatter light. The aperture ratio should be similar to the previous case (~90%).
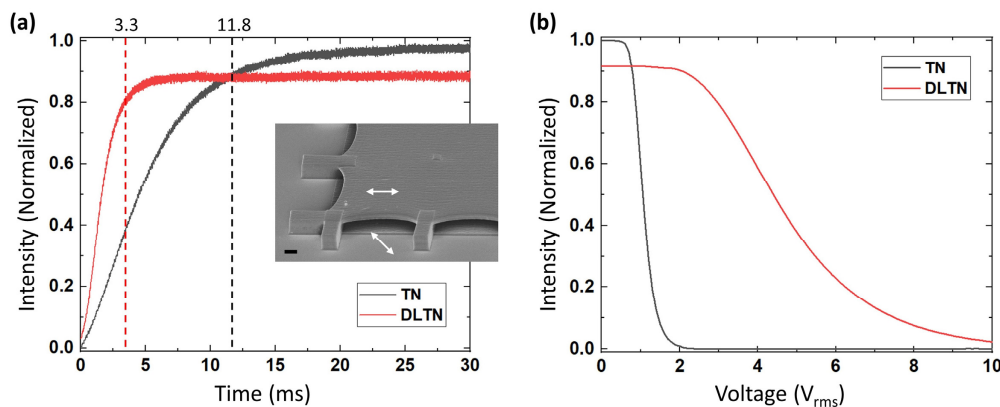
Fig. 12. A dual-layer TN sample compared to a conventional single-layer TN sample with the same total effective LC thickness of 3.3 µm. (a) The relaxation time (intensity change from 100% to 10% when releasing from 10 V_{rms}) of dual- and single-layer TN samples are 3.3 ms and 11.8 ms, respectively. Inset: the SEM image of a two-layer scaffold, scale bar: 2 µm. The white arrows denote the alignment direction at each layer. (b) The measured voltage-dependent transmittance changes of the dual-layer and single-layer TN samples at $\lambda = 633$ nm.

Apart from dual-layer LC devices, for phase modulators to work at longer wavelengths while keeping similar response time, more sub-layers can be established to achieve adequate phase change. Figure 13 depicts the SEM images of a four-layer scaffold for a phase modulator. It is in general feasible to build more layers. However, there are some other concerns such as polymer shrinkage after polymerization and sub-layer thickness control, which will be discussed later.
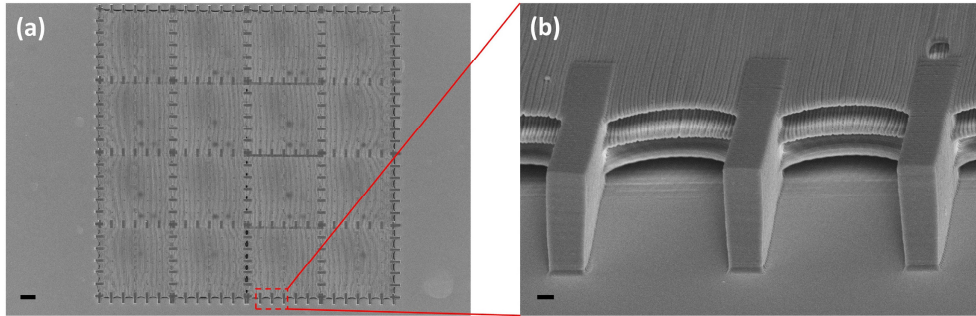

Fig. 13. SEM images of a four-layer scaffold for a phase modulator: (a) Top view and (b) side view. From the side view, it can be clearly distinguished that there are three polymer layers. Scale bar: 20 µm (a) and 2 µm (b).

So far, we have focused on simple multi-layer structure where each layer provides uniform LC alignment. By designing it into a space-variant fashion, more device functions can be fulfilled. Here, we propose a novel, ultra-broadband beam steering device, namely twisted-nematic diffractive waveplate (TNDW) that in principle can be achieved through TPP.

TN LCD [103] has been widely used in notebook computers because of its high transmittance and high fabrication yield. In a TN cell, the unique adiabatic following (or wave-guiding) effect occurs when the incident light traverses through the LC layer, in the limit of a slow twist of LC director [7], also known as Mauguin condition:

$$\phi_{\text{twist}} << \frac{\Gamma}{2} = \frac{\pi \cdot \Delta n \cdot d}{\lambda}, \tag{5}$$

where ϕ_{twist} stands for the LC twist angle and Γ is the phase retardation. Under the Mauguin condition, the linear polarization direction would basically follow the LC directors when the incident light is linearly polarized. Therefore, we can utilize such a polarization rotation effect to modulate the output polarization state and generate geometric phase delay. Especially, adiabatic following is insensitive to the wavelength, which contributes to the achromatic performance of TN mode. In our proposed TNDW, the LC director distribution within one pitch follows:

$$\phi_{\text{LC}} = 2\pi \frac{z}{d} \frac{x}{p}, \tag{6}$$

where $x \in [0, p]$, $z \in [0, d]$, d is the effective total LC thickness and p is the pitch length along x-direction.

The schematic diagram of the device configuration is illustrated as Fig. 14. To achieve the smooth TN alignment along z direction, we propose to add a floating alignment layer using TPP. So, there are three surface alignment layers in the proposed diffractive waveplate. The bottom surface provides a homogenous alignment anchoring. The top surface alignment

direction follows a cycloidal profile with $2\pi x/p$ and the floating alignment follows $\pi x/p$, as Fig. 14 presents.
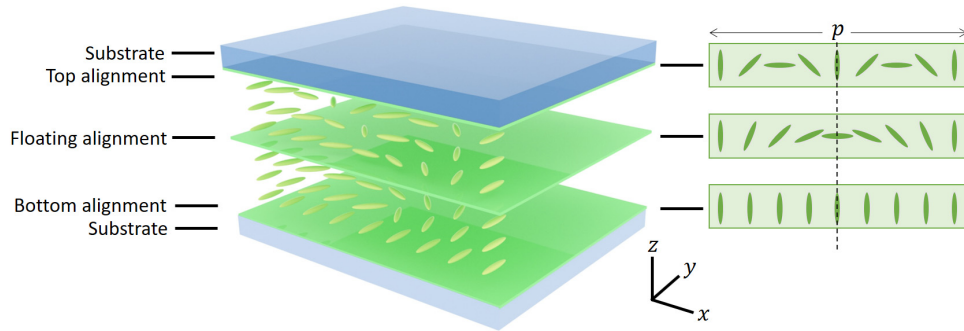

Fig. 14. The schematic diagram of the proposed twisted-nematic diffractive waveplate with an additional floating alignment layer enabled by two photon polymerization.
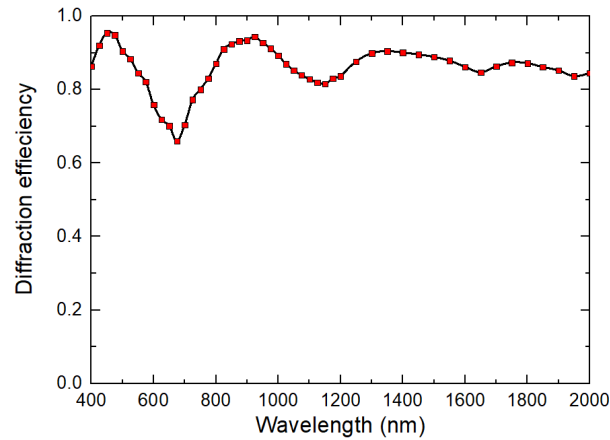

Fig. 15. Simulated diffraction efficiency for a TN diffractive waveplate with circularly polarized incident light.

With Mauguin limit [Eq. (5)] fulfilled, more detailed analytical deviations can be carried out based on Jones matrix and far-field Fourier transformation. For a circularly polarized light incident from homogenous alignment layer, namely bottom alignment in Fig. 14, the output far-field electrical distribution can be written as:

$$\begin{bmatrix} E_x \\ E_y \end{bmatrix} = \frac{1}{\sqrt{2}} \cos\left(\frac{\Gamma}{2}\right) \begin{bmatrix} 1 \\ i \end{bmatrix} e^{i\pi x/p} - \frac{1}{\sqrt{2}} \sin\left(\frac{\Gamma}{2}\right) \begin{bmatrix} i \\ 1 \end{bmatrix} e^{-i\pi x/p}. \tag{7}$$

It is easy to find that the diffraction efficiency of ± 1 orders are dependent on the phase retardation Γ. While if the circularly polarized light incident from top alignment in Fig. 14, the output is:

$$\begin{bmatrix} E_x \\ E_y \end{bmatrix} = \frac{1}{\sqrt{2}} \begin{bmatrix} e^{-i\Gamma/2} \\ -ie^{i\Gamma/2} \end{bmatrix} \cdot e^{i\pi x/p}. \tag{8}$$

Interestingly, only + 1 order exists with ~100% diffraction efficiency in theory, as Eq. (8) clearly illustrates. Thus, a broadband diffractive waveplate can be achieved by utilizing the polarization rotation effect. Some preliminary optical simulations were carried out with finite-element method (FEM). We simulated a TNDW with pitch length $p = 45$ μm, LC layer

thickness d = 15 μm and LC birefringence Δn = 0.3 as an example. The simulated diffraction efficiency is plotted in Fig. 15. Over 80% efficiency has been achieved for an ultra-broad wavelength range from visible to near IR. The diffraction efficiency does not reach the theoretical value 100% in that the diffraction and refractive effects are ignored in the calculations, and there is also disclination line located at $x = p/2$. The results presented in Fig. 15 demonstrate the achromatic behavior of the TNDW. Comparing to previous multi-twist designs and active diffractive waveplates (or polarization gratings) [10,11,77,78,104–106], our device offers an ultra-broadband operation window while keeping its active switching capability.

Beside multi-layer structures, TPP has also been utilized to create other 3D structures that show fascinating stimuli-driven responses when combined with LCs. For instance, memory effect was revealed in 3D micro-lattices filled with LCs [107] and controllable light diffraction was explored in woodpile photonic crystals assisted by LCs [108]. LC, not limited to nematc phase, as a general multi-response material should find abundant research opportunities in stimuli-responsive devices [109].

4. Direct-laser writing on liquid-crystal monomers

In Sec. 3, we emphasize on TPP for LC alignment. As an important and rising research direction, DLW on LC mixtures has inspired a great deal of interests. The basic working principle and configurations for DLW on LC monomers are the same as those mentioned in Sec. 2. However, in this case, at least a portion of the photoresist materials has liquid-crystalline phase (usually reactive mesogens).

Previous studies of LC elastomers/networks have been focused on relatively simple structures [40,110]. The advent of TPP DLW technique would further enrich the design of sophisticated tunable and functional LC elastomer-based devices. In the very early stage, TPP was applied to create micropatterns and variable-step gratings in nematic elastomers [111]. Such a grating period changes with the temperature. Compared to single-photon excitation, TPP yields finer patterns. Later in 2014, the 3D capabilities of DLW in LC elastomers were explored [112]. By demonstrating polymerized lines, rings and woodpiles structures, Zeng et al. showed that TPP DLW is suitable for fabricating 1D, 2D, and 3D LC elastomer structures with sub-micrometer resolution. The polymerized structures maintain the pre-defined (rubbed alignment) molecular orientation and exhibit swelling perpendicular to the alignment direction. By now, DLW on LC elastomers or networks have accomplished light-activated micro-walkers [113], micro-hand [114], micro-actuator with non-reciprocal motion [115], suspended micromembranes [116], and light-controlled 2D grating [117], photonic circuits [118], elastic microcavities [119], etc. Other attempts on photoresist materials development and writing condition discussion promote the combination of TPP with LCs further [120–122].

Beside LC elastomers, DLW has also been successfully applied to functionalize other LC devices. A comprehensive work illustrated that DLW can be utilized to generate local defect and control the local pitch length in cholesteric LCs (CLCs) [123]. These functional CLCs are promising for low-threshold lasing and multicolor reflections. Another study showed that DLW can generate localized polymer networks in chiral nematic LCs such that uniform lying helix (ULH) state can be spontaneously formed [124]. In a very recent report, DLW was employed to generating images and identification codes in LC device [125]. An image can be recorded by locally polymerizing reactive mesogens at a certain voltage. After polymerization, the image can be read out at other voltages and erased by the recording voltage. With this concept, Tartan et al. also demonstrated a multi-step polymerized pattern where different part of the pattern was polymerized at a different voltage. The readout images can be changed at different voltages.

5. Some design challenges and considerations

5.1 Fabrication yield

The designs of abovementioned LC devices are only tested in lab, in which fabrication yield is not a concern. However, when pursuing for large-area devices, the DLW process is time-consuming because it is intrinsically a serial process. For instance, after a first-order optimization of writing parameters, a throughput of 0.01 in^2/hr was reported for writing a dual-layer phase modulator scaffold [126]. To overcome this bottleneck, many methods have been proposed, such as using holographic components and spatial light modulators [56,127–129]. The basic idea is to turn the serial process into parallel process, and this works for all cases (2D, 2.5D and 3D structures). In particular, for 2D structures, other technique such as NIL can assist to improve the fabrication yield while maintaining high quality and good reliability.

5.2 Polymer relaxation/deformation

As mentioned in Sec. 3.3, when constructing more layers in a phase modulator, polymer shrinkage can be a potential issue. As an example, Fig. 16 demonstrates a peeled-off four-layer phase modulator scaffold due to the relaxation of polymerized photoresist. With the same polymer pillar/supporter parameters, dual- and three-layer scaffolds can withstand the residue stress after polymerization. To avoid peeling off or other polymer deformation (such as curved edges), stronger supporter can be designed, often in cost of the size of effective area (aperture ratio). This is not a special case but rather general [130]. Other strategies to correct this problem are through chemical group engineering of photoresists [131] and geometrical pre-compensation of the expected deformations [132]. Interestingly, the residue stress that is detrimental for fabrication of 3D structures can be harnessed to create 3D geometries from 2D patterns [133]. By investigating the residue stress in terms of polymerized layer number, it has been demonstrated that the polymer self-bending can be designed to create different shapes of lotus flower as well as a shark skin-like geometry.
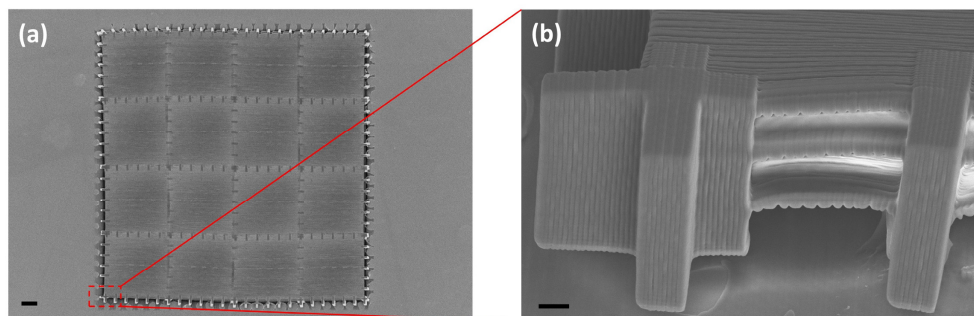
Fig. 16. SEM images of a peeled-off four-layer scaffold for a phase modulator: (a) Top view and (b) side view. Scale bar: 20 μm (a) and 2 μm (b).

6. Conclusion

We have briefly reviewed the recent advances in TPP DLW-assisted LC devices. Taking the advantages of high-resolution 3D fabrication, TPP is able to generate LC alignment based on surface morphology easily. These alignment patterns can be created on planar, curvilinear surfaces, and especially in a 3D volume. Specifically, for planar surface alignment, we started from demonstrating simple orthogonal-direction patterned alignment for LC binary gratings. Then, through an example of PB microlens array, the feasibility of arbitrary-direction alignment patterning was proven. Through modifying the geometry of surface morphology, degenerate LC alignment can also be accomplished. Then, we discussed the viability of

creating alignment on curvilinear surfaces via an instance of refractive microlens arrays. Unlike traditional method, TPP is capable of polymerizing both microlenses and alignment simultaneously with high quality. Next, we highlighted the unique feature of TPP that is to construct LC alignment in a 3D volume. We began the discussion with simple multi-layer structures that can be used for achieving fast response time and polarization-independent functions. Then, based on these results, we proposed a novel, ultra-broadband, switchable TNDW that provides over 80% diffraction efficiency spanning from the visible to near IR spectral region. Other than multi-layer structures, photonic crystals- and 3D microlattices-based tunable devices have also illustrated interdisciplinary-study possibilities. Besides using TPP to fabricate LC alignment, direct writing on LC mixtures opens other arenas. Functional and responsive devices have been demonstrated by structured LC elastomers/networks. Moreover, the specially engineered defects in LC cells also give rise to novel device functions. Lastly, we point out two technical issues for future researches: fabrication yield and polymer relaxation/deformation. As TPP is intrinsically a serial process, the fabrication yield for large area can be low. To overcome this issue, turning the serial process to parallel one is crucial. Another aspect, post-polymerization deformation of the photoresist, should also be considered during designs. As the advances in fabrication technique will bring in new possibilities, we believe TPP-based DLW can achieve more novel, tunable LC photonic devices in the near future.

Funding

Acknowledgments

References

1. T. Kato, N. Mizoshita, and K. Kishimoto, "Functional liquid-crystalline assemblies: self-organized soft materials," Angew. Chem. Int. Ed. Engl. **45**(1), 38–68 (2005).
2. S. J. Woltman, G. D. Jay, and G. P. Crawford, "Liquid-crystal materials find a new order in biomedical applications," Nat. Mater. **6**(12), 929–938 (2007).
3. D.-K. Yang and S.-T. Wu, *Fundamentals of Liquid Crystal Devices* (John Wiley & Sons, 2006).
4. L. M. Blinov and V. G. Chigrinov, *Electrooptic Effects in Liquid Crystal Materials* (Springer, 1994).
5. H. K. Bisoyi and Q. Li, "Light-driven liquid crystalline materials: from photo-induced phase transitions and property modulations to applications," Chem. Rev. **116**(24), 15089–15166 (2016).
6. R. Chen, Y. H. Lee, T. Zhan, K. Yin, Z. An, and S. T. Wu, "Multi-stimuli-responsive self-organized liquid crystal Bragg gratings," Adv. Opt. Mater. **7**, 1900101 (2019).
7. S. T. Wu and D. K. Yang, *Reflective Liquid Crystal Displays* (Wiley, 2001).
8. H. W. Chen, J. H. Lee, B. Y. Lin, S. Chen, and S. T. Wu, "Liquid crystal display and organic light-emitting diode display: present status and future perspectives," Light Sci. Appl. **7**(3), 17168 (2018).
9. S. Serak, N. Tabiryan, and B. Zeldovich, "High-efficiency 1.5 microm thick optical axis grating and its use for laser beam combining," Opt. Lett. **32**(2), 169–171 (2007).
10. H. Sarkissian, S. V. Serak, N. V. Tabiryan, L. B. Glebov, V. Rotar, and B. Y. Zeldovich, "Polarization-controlled switching between diffraction orders in transverse-periodically aligned nematic liquid crystals," Opt. Lett. **31**(15), 2248–2250 (2006).
11. K. Yin, Y. H. Lee, Z. He, and S. T. Wu, "Stretchable, flexible, rollable, and adherable polarization volume grating film," Opt. Express **27**(4), 5814–5823 (2019).
12. K. Hirabayashi and T. Kurokawa, "Liquid crystal devices for optical communication and information processing systems," Liq. Cryst. **14**(2), 307–317 (1993).
13. A. D'Alessandro and R. Asquini, "Liquid crystal devices for photonic switching applications: state of the art and future developments," Mol. Cryst. Liq. Cryst. (Phila. Pa.) **398**(1), 207–221 (2003).
14. F. Du, Y. Q. Lu, and S. T. Wu, "Electrically tunable liquid-crystal photonic crystal fiber," Appl. Phys. Lett. **85**(12), 2181–2183 (2004).
15. H. Chen, Z. Luo, R. Zhu, Q. Hong, and S. T. Wu, "Tuning the correlated color temperature of white LED with a guest-host liquid crystal," Opt. Express **23**(10), 13060–13068 (2015).

16. C.-C. Huang, Y.-Y. Kuo, S.-H. Chen, W.-T. Chen, and C.-Y. Chao, "Liquid-crystal-modulated correlated color temperature tunable light-emitting diode with highly accurate regulation," Opt. Express **23**(3), A149–A156 (2015).

17. Z. He, H. Chen, Y. H. Lee, and S. T. Wu, "Tuning the correlated color temperature of white light-emitting diodes resembling Planckian locus," Opt. Express **26**(2), A136–A143 (2018).

18. R. A. M. Hikmet and H. Kemperman, "Electrically switchable mirrors and optical components made from liquid-crystal gels," Nature **392**(6675), 476–479 (1998).

19. D. Cupelli, F. P. Nicoletta, S. Manfredi, M. Vivacqua, P. Formoso, G. De Filpo, and G. Chidichimo, "Self-adjusting smart windows based on polymer-dispersed liquid crystals," Sol. Energy Mater. Sol. Cells **93**(11), 2008–2012 (2009).

20. M. Kim, K. J. Park, S. Seok, J. M. Ok, H.-T. Jung, J. Choe, D. H. Oh, and D. H. Kim, "Fabrication of microcapsules for dye-doped polymer-dispersed liquid crystal-based smart windows," ACS Appl. Mater. Interfaces **7**(32), 17904–17909 (2015).

21. J. Sautter, I. Staude, M. Decker, E. Rusak, D. N. Neshev, I. Brener, and Y. S. Kivshar, "Active tuning of all-dielectric metasurfaces," ACS Nano **9**(4), 4308–4315 (2015).

22. Y. J. Liu, G. Y. Si, E. S. P. Leong, N. Xiang, A. J. Danner, and J. H. Teng, "Light-driven plasmonic color filters by overlaying photoresponsive liquid crystals on gold annular aperture arrays," Adv. Mater. **24**(23), OP131–OP135 (2012).

23. A. Komar, Z. Fang, J. Bohn, J. Sautter, M. Decker, A. Miroshnichenko, T. Pertsch, I. Brener, Y. Kivshar, I. Staude, and D. Neshev, "Electrically tunable all-dielectric optical metasurfaces based on liquid crystals," Appl. Phys. Lett. **110**(7), 071109 (2017).

24. Y. H. Lee, G. Tan, T. Zhan, Y. Weng, G. Liu, F. Gou, F. Peng, N. V. Tabiryan, S. Gauza, and S. T. Wu, "Recent progress in Pancharatnam-Berry phase optical elements and the applications for virtual/augmented realities," Opt. Data Process. Storage **3**(1), 79–88 (2017).

25. T. Zhan, Y. H. Lee, and S. T. Wu, "High-resolution additive light field near-eye display by switchable Pancharatnam-Berry phase lenses," Opt. Express **26**(4), 4863–4872 (2018).

26. Y. Weng, Y. Zhang, J. Cui, A. Liu, Z. Shen, X. Li, and B. Wang, "Liquid-crystal-based polarization volume grating applied for full-color waveguide displays," Opt. Lett. **43**(23), 5773–5776 (2018).

27. M. Schadt, K. Schmitt, V. Kozinkov, and V. Chigrinov, "Surface-induced parallel alignment of liquid crystals by linearly polymerized photopolymers," Jpn. J. Appl. Phys. **31**(7), 2155–2164 (1992).

28. O. Yaroshchuk and Y. Reznikov, "Photoalignment of liquid crystals: basics and current trends," J. Mater. Chem. **22**(2), 286–300 (2012).

29. V. G. Chigrinov, V. M. Kozenkov, and H.-S. Kwok, *Photoalignment of Liquid Crystalline Materials: Physics and Applications* (Wiley, 2008).

30. H. Finkelmann, H. Kock, and G. Rehage, "Investigations on LC polysiloxanes 3. Liquid crystalline elastomers - a new type of liquid crystalline material," Makromol. Chem., Rapid. Commun. **2**(4), 317–322 (1981).

31. M. Warner and E. M. Terentjev, *Liquid Crystal Elastomers* (Oxford University, 2007).

32. W. H. de Jeu, *Liquid Crystal Elastomers: Materials and Applications* (Springer, 2012).

33. T. J. White and D. J. Broer, "Programmable and adaptive mechanics with liquid crystal polymer networks and elastomers," Nat. Mater. **14**(11), 1087–1098 (2015).

34. C. Ohm, M. Brehmer, and R. Zentel, "Liquid crystalline elastomers as actuators and sensors," Adv. Mater. **22**(31), 3366–3387 (2010).

35. Y. Yu and T. Ikeda, "Soft actuators based on liquid-crystalline elastomers," Angew. Chem. Int. Ed. Engl. **45**(33), 5416–5418 (2006).

36. P. G. de Gennes, "Réflexions sur un type de polymères nématiques," CR Acad. Sci. Ser., B **B281**, 101–103 (1975).

37. M. Yamada, M. Kondo, R. Miyasato, Y. Naka, J. I. Mamiya, M. Kinoshita, A. Shishido, Y. Yu, C. J. Barrett, and T. Ikeda, "Photomobile polymer materials—various three-dimensional movements," J. Mater. Chem. **19**(1), 60–62 (2009).

38. Y. Yu, M. Nakano, and T. Ikeda, "Photomechanics: directed bending of a polymer film by light," Nature **425**(6954), 145 (2003).

39. A. H. Gelebart, D. Jan Mulder, M. Varga, A. Konya, G. Vantomme, E. W. Meijer, R. L. B. Selinger, and D. J. Broer, "Making waves in a photoactive polymer film," Nature **546**(7660), 632–636 (2017).

40. S. Nocentini, C. Parmeggiani, D. Martella, and D. S. Wiersma, "Optically driven soft micro robotics," Adv. Opt. Mater. **6**(14), 1800207 (2018).

41. H. Shahsavan, L. Yu, A. Jákli, and B. Zhao, "Smart biomimetic micro/nanostructures based on liquid crystal elastomers and networks," Soft Matter **13**(44), 8006–8022 (2017).

42. D. Martella, S. Nocentini, C. Parmeggiani, and D. S. Wiersma, "Self-regulating capabilities in photonic robotics," Adv. Mater. Technol. **4**(2), 1800571 (2018).

43. H. Kumagai, K. Midorikawa, K. Toyoda, S. Nakamura, T. Okamoto, and M. Obara, "Ablation of polymer films by a femtosecond high-peak-power Ti:sapphire laser at 798 nm," Appl. Phys. Lett. **65**(14), 1850–1852 (1994).

44. K. M. Davis, K. Miura, N. Sugimoto, and K. Hirao, "Writing waveguides in glass with a femtosecond laser," Opt. Lett. **21**(21), 1729–1731 (1996).

45. S. Maruo, O. Nakamura, and S. Kawata, "Three-dimensional microfabrication with two-photon-absorbed photopolymerization," Opt. Lett. **22**(2), 132–134 (1997).

46. B. H. Cumpston, S. P. Ananthavel, S. Barlow, D. L. Dyer, J. E. Ehrlich, L. L. Erskine, A. A. Heikal, S. M. Kuebler, I.-Y. S. Lee, D. McCord-Maughon, J. Qin, H. Röckel, M. Rumi, X.-L. Wu, S. R. Marder, and J. W. Perry, "Two-photon polymerization initiators for three-dimensional optical data storage and microfabrication," Nature **398**(6722), 51–54 (1999).
47. S. Kawata, H.-B. Sun, T. Tanaka, and K. Takada, "Finer features for functional microdevices," Nature **412**(6848), 697–698 (2001).
48. J. Serbin, A. Egbert, A. Ostendorf, B. N. Chichkov, R. Houbertz, G. Domann, J. Schulz, C. Cronauer, L. Fröhlich, and M. Popall, "Femtosecond laser-induced two-photon polymerization of inorganic-organic hybrid materials for applications in photonics," Opt. Lett. **28**(5), 301–303 (2003).
49. J. L. Digaum, J. J. Pazos, J. Chiles, J. D'Archangel, G. Padilla, A. Tatulian, R. C. Rumpf, S. Fathpour, G. D. Boreman, and S. M. Kuebler, "Tight control of light beams in photonic crystals with spatially-variant lattice orientation," Opt. Express **22**(21), 25788–25804 (2014).
50. T. Bückmann, N. Stenger, M. Kadic, J. Kaschke, A. Frölich, T. Kennerknecht, C. Eberl, M. Thiel, and M. Wegener, "Tailored 3D mechanical metamaterials made by dip-in direct-laser-writing optical lithography," Adv. Mater. **24**(20), 2710–2714 (2012).
51. F. Klein, B. Richter, T. Striebel, C. M. Franz, G. von Freymann, M. Wegener, and M. Bastmeyer, "Two-component polymer scaffolds for controlled three-dimensional cell culture," Adv. Mater. **23**(11), 1341–1345 (2011).
52. P. I. Dietrich, M. Blaicher, I. Reuter, M. Billah, T. Hoose, A. Hofmann, C. Caer, R. Dangel, B. Offrein, U. Troppenz, M. Moehrle, W. Freude, and C. Koos, "In situ 3D nanoprinting of free-form coupling elements for hybrid photonic integration," Nat. Photonics **12**(4), 241–247 (2018).
53. M. Pawlicki, H. A. Collins, R. G. Denning, and H. L. Anderson, "Two-photon absorption and the design of two-photon dyes," Angew. Chem. Int. Ed. Engl. **48**(18), 3244–3266 (2009).
54. W. Haske, V. W. Chen, J. M. Hales, W. Dong, S. Barlow, S. R. Marder, and J. W. Perry, "65 nm feature sizes using visible wavelength 3-D multiphoton lithography," Opt. Express **15**(6), 3426–3436 (2007).
55. K. Obata, A. El-Tamer, L. Koch, U. Hinze, and B. N. Chichkov, "High-aspect 3D two-photon polymerization structuring with widened objective working range (WOW-2PP)," Light Sci. Appl. **2**(12), e116 (2013).
56. J. K. Hohmann, M. Renner, E. H. Waller, and G. von Freymann, "Three-Dimensional μ-Printing: an enabling technology," Adv. Opt. Mater. **3**(11), 1488–1507 (2015).
57. C.-H. Lee, H. Yoshida, Y. Miura, A. Fujii, and M. Ozaki, "Local liquid crystal alignment on patterned micrograting structures photofabricated by two photon excitation direct laser writing," Appl. Phys. Lett. **93**(17), 173509 (2008).
58. Z. Ji, X. Zhang, B. Shi, W. Li, W. Luo, I. Drevensek-Olenik, Q. Wu, and J. Xu, "Compartmentalized liquid crystal alignment induced by sparse polymer ribbons with surface relief gratings," Opt. Lett. **41**(2), 336–339 (2016).
59. G. Carbone, D. Corbett, S. J. Elston, P. Raynes, A. Jesacher, R. Simmonds, and M. Booth, "Uniform lying helix alignment on periodic surface relief structure generated via laser scanning lithography," Mol. Cryst. Liq. Cryst. (Phila. Pa.) **544**(1), 37–1025 (2011).
60. H. Zeng, P. Wasylczyk, G. Cerretti, D. Martella, C. Parmeggiani, and D. S. Wiersma, "Alignment engineering in liquid crystalline elastomers: free-form microstructures with multiple functionalities," Appl. Phys. Lett. **106**(11), 111902 (2015).
61. J. D. Lin, Y. L. Daniel Ho, L. Chen, M. Lopez-Garcia, S. A. Jiang, M. P. C. Taverne, C. R. Lee, and J. G. Rarity, "Microstructure-stabilized blue phase liquid crystals," ACS Omega **3**(11), 15435–15441 (2018).
62. S. R. Nersisyan, N. V. Tabiryan, D. M. Steeves, and B. R. Kimball, "Optical axis gratings in liquid crystals and their use for polarization insensitive optical switching," J. Nonlinear Opt. Phys. Mater. **18**(01), 1–47 (2009).
63. H. W. Chen, R. D. Zhu, J. He, W. Duan, W. Hu, Y. Q. Lu, M. C. Li, S. L. Lee, Y. J. Dong, and S. T. Wu, "Going beyond the limit of an LCD's color gamut," Light Sci. Appl. **6**(9), e17043 (2017).
64. B. Wen, R. G. Petschek, and C. Rosenblatt, "Nematic liquid-crystal polarization gratings by modification of surface alignment," Appl. Opt. **41**(7), 1246–1250 (2002).
65. J. Chen, P. J. Bos, H. Vithana, and D. L. Johnson, "An electrooptically controlled liquid crystal diffraction grating," Appl. Phys. Lett. **67**(18), 2588–2590 (1995).
66. W. M. Gibbons and S. T. Sun, "Optically generated liquid crystal gratings," Appl. Phys. Lett. **65**(20), 2542–2544 (1994).
67. W. Hu, A. Kumar Srivastava, X. W. Lin, X. Liang, Z. J. Wu, J. T. Sun, G. Zhu, V. Chigrinov, and Y. Q. Lu, "Polarization independent liquid crystal gratings based on orthogonal photoalignments," Appl. Phys. Lett. **100**(11), 111116 (2012).
68. W. Hu, A. Srivastava, F. Xu, J. T. Sun, X. W. Lin, H. Q. Cui, V. Chigrinov, and Y. Q. Lu, "Liquid crystal gratings based on alternate TN and PA photoalignment," Opt. Express **20**(5), 5384–5391 (2012).
69. V. Kapoustine, A. Kazakevitch, V. So, and R. Tam, "Simple method of formation of switchable liquid crystal gratings by introducing periodic photoalignment pattern into liquid crystal cell," Opt. Commun. **266**(1), 1–5 (2006).
70. M. Schadt and W. Helfrich, "Voltage-dependent optical activity of a twisted nematic liquid crystal," Appl. Phys. Lett. **18**(4), 127–128 (1971).
71. Z. He, Y. H. Lee, R. Chen, D. Chanda, and S. T. Wu, "Switchable Pancharatnam-Berry microlens array with nano-imprinted liquid crystal alignment," Opt. Lett. **43**(20), 5062–5065 (2018).

72. S. Pancharatnam, "Generalized theory of interference and its applications," Proc. Indian Acad. Sci. Sect. A Phys. Sci. **44**(6), 398–417 (1956).
73. M. V. Berry, "Quantal phase factors accompanying adiabatic changes," Proc. R. Soc. Lond. A Phys. Sci. **392**(1802), 45–57 (1984).
74. S. Y. Chou, P. R. Krauss, and P. J. Renstrom, "Imprint lithography with 25-nanometer resolution," Science **272**(5258), 85–87 (1996).
75. Y. Yi, M. Nakata, A. R. Martin, and N. A. Clark, "Alignment of liquid crystals by topographically patterned polymer films prepared by nanoimprint lithography," Appl. Phys. Lett. **90**(16), 163510 (2007).
76. H. G. Park, J. J. Lee, K. Y. Dong, B. Y. Oh, Y. H. Kim, H. Y. Jeong, B. K. Ju, and D. S. Seo, "Homeotropic alignment of liquid crystals on a nano-patterned polyimide surface using nanoimprint lithography," Soft Matter **7**(12), 5610–5614 (2011).
77. C. Oh and M. J. Escuti, "Achromatic diffraction from polarization gratings with high efficiency," Opt. Lett. **33**(20), 2287–2289 (2008).
78. K. Gao, C. McGinty, H. Payson, S. Berry, J. Vornehm, V. Finnemeyer, B. Roberts, and P. Bos, "High-efficiency large-angle Pancharatnam phase deflector based on dual-twist design," Opt. Express **25**(6), 6283–6293 (2017).
79. J. Kim, Y. Li, M. N. Miskiewicz, C. Oh, M. W. Kudenov, and M. J. Escuti, "Fabrication of ideal geometric-phase holograms with arbitrary wavefronts," Optica **2**(11), 958–964 (2015).
80. F. Gou, F. Peng, Q. Ru, Y.-H. Lee, H. Chen, Z. He, T. Zhan, K. L. Vodopyanov, and S.-T. Wu, "Mid-wave infrared beam steering based on high-efficiency liquid crystal diffractive waveplates," Opt. Express **25**(19), 22404–22410 (2017).
81. E. Hasman, V. Kleiner, G. Biener, and A. Niv, "Polarization dependent focusing lens by use of quantized PancharatnamBerry phase diffractive optics," Appl. Phys. Lett. **82**(3), 328–330 (2003).
82. S. C. McEldowney, D. M. Shemo, R. A. Chipman, and P. K. Smith, "Creating vortex retarders using photoaligned liquid crystal polymers," Opt. Lett. **33**(2), 134–136 (2008).
83. D. Mawet, E. Serabyn, K. Liewer, Ch. Hanot, S. McEldowney, D. Shemo, and N. O'Brien, "Optical Vectorial Vortex Coronagraphs using Liquid Crystal Polymers: theory, manufacturing and laboratory demonstration," Opt. Express **17**(3), 1902–1918 (2009).
84. W. Ji, C. H. Lee, P. Chen, W. Hu, Y. Ming, L. Zhang, T. H. Lin, V. Chigrinov, and Y. Q. Lu, "Meta-q-plate for complex beam shaping," Sci. Rep. **6**(1), 25528 (2016).
85. C. Tsakonas, A. J. Davidson, C. V. Brown, and N. J. Mottram, "Multistable alignment states in nematic liquid crystal filled well," Appl. Phys. Lett. **90**(11), 111913 (2007).
86. J. H. Kim, M. Yoneya, and H. Yokoyama, "Tristable nematic liquid-crystal device using micropatterned surface alignment," Nature **420**(6912), 159–162 (2002).
87. D. Franklin, Y. Chen, A. Vázquez-Guardado, S. Modak, J. Boroumand, D. Xu, S. T. Wu, and D. Chanda, "Polarization-independent actively tunable colour generation on imprinted plasmonic surfaces," Nat. Commun. **6**(1), 7337 (2015).
88. D. Franklin, R. Frank, S. T. Wu, and D. Chanda, "Actively addressed single pixel full-colour plasmonic display," Nat. Commun. **8**, 15209 (2017).
89. A. Orth and K. Crozier, "Microscopy with microlens arrays: high throughput, high resolution and light-field imaging," Opt. Express **20**(12), 13522–13531 (2012).
90. Y. H. Lin, Y. J. Wang, and V. Reshetnyak, "Liquid crystal lenses with tunable focal length," Liq. Cryst. Rev. **5**(2), 111–143 (2017).
91. S. Masuda, S. Takahashi, T. Nose, S. Sato, and H. Ito, "Liquid-crystal microlens with a beam-steering function," Appl. Opt. **36**(20), 4772–4778 (1997).
92. A. Akatay, C. Ataman, and H. Urey, "High-resolution beam steering using microlens arrays," Opt. Lett. **31**(19), 2861–2863 (2006).
93. L. Hu, L. Xuan, D. Li, Z. Cao, Q. Mu, Y. Liu, Z. Peng, and X. Lu, "Wavefront correction based on a reflective liquid crystal wavefront sensor," J. Opt. A, Pure Appl. Opt. **11**(1), 015511 (2009).
94. J.-H. Na, S.-C. Park, S.-U. Kim, Y. Choi, and S.-D. Lee, "Physical mechanism for flat-to-lenticular lens conversion in homogeneous liquid crystal cell with periodically undulated electrode," Opt. Express **20**(2), 864–869 (2012).
95. S. Sato, "Liquid-crystal lens-cells with variable focal length," Jpn. J. Appl. Phys. **18**(9), 1679–1684 (1979).
96. Z. He, Y. H. Lee, D. Chanda, and S. T. Wu, "Adaptive liquid crystal microlens array enabled by two-photon polymerization," Opt. Express **26**(16), 21184–21193 (2018).
97. Y. H. Lee, D. Franklin, F. Gou, G. Liu, F. Peng, D. Chanda, and S. T. Wu, "Two-photon polymerization enabled multi-layer liquid crystal phase modulator," Sci. Rep. **7**(1), 16260 (2017).
98. R. M. Hyman, A. Lorenz, S. M. Morris, and T. D. Wilkinson, "Polarization-independent phase modulation using a blue-phase liquid crystal over silicon device," Appl. Opt. **53**(29), 6925–6929 (2014).
99. D. E. Lucchetta, R. Karapinar, A. Manni, and F. Simoni, "Phase-only modulation by nanosized polymerdispersed liquid crystals," J. Appl. Phys. **91**(9), 6060–6065 (2002).
100. Y. Huang, C.-H. Wen, and S.-T. Wu, "Polarization-independent and submillisecond response phase modulators using a 90° twisted dual-frequency liquid crystal," Appl. Phys. Lett. **89**(2), 021103 (2006).
101. Y.-H. Lin, H. Ren, Y.-H. Wu, Y. Zhao, J. Fang, Z. Ge, and S.-T. Wu, "Polarization-independent liquid crystal phase modulator using a thin polymer-separated double-layered structure," Opt. Express **13**(22), 8746–8752 (2005).

102. Z. He, Y. H. Lee, F. Gou, D. Franklin, D. Chanda, and S. T. Wu, "Polarization-independent phase modulators enabled by two-photon polymerization," Opt. Express **25**(26), 33688–33694 (2017).
103. M. Schadt, "Milestone in the history of field-effect liquid crystal displays and materials," Jpn. J. Appl. Phys. **48**(3), 03B001 (2009).
104. R. K. Komanduri, K. F. Lawler, and M. J. Escuti, "Multi-twist retarders: broadband retardation control using self-aligning reactive liquid crystal layers," Opt. Express **21**(1), 404–420 (2013).
105. C. Provenzano, P. Pagliusi, and G. Cipparrone, "Highly efficient liquid crystal based diffraction grating induced by polarization holograms at the aligning surfaces," Appl. Phys. Lett. **89**(12), 121105 (2006).
106. H. Chen, Y. Weng, D. Xu, N. V. Tabiryan, and S. T. Wu, "Beam steering for virtual/augmented reality displays with a cycloidal diffractive waveplate," Opt. Express **24**(7), 7287–7298 (2016).
107. F. Serra, S. M. Eaton, R. Cerbino, M. Buscaglia, G. Cerullo, R. Osellame, and T. Bellini, "Nematic liquid crystals embedded in cubic microlattices: memory effects and bistable pixels," Adv. Funct. Mater. **23**(32), 3990–3994 (2013).
108. C. H. Ho, Y. C. Cheng, L. Maigyte, H. Zeng, J. Trull, C. Cojocaru, D. S. Wiersma, and K. Staliunas, "Controllable light diffraction in woodpile photonic crystals filled with liquid crystal," Appl. Phys. Lett. **106**(2), 021113 (2015).
109. V. G. Chigrinov, *Liquid Crystal Photonics* (Nova, 2014).
110. B. A. Kowalski, T. C. Guin, A. D. Auguste, N. P. Godman, and T. J. White, "Pixelated polymers: directed self assembly of liquid crystalline polymer networks," ACS Macro Lett. **6**(4), 436–441 (2017).
111. E. Sungur, M. H. Li, G. Taupier, A. Boeglin, M. Romeo, S. Méry, P. Keller, and K. D. Dorkenoo, "External stimulus driven variable-step grating in a nematic elastomer," Opt. Express **15**(11), 6784–6789 (2007).
112. H. Zeng, D. Martella, P. Wasylczyk, G. Cerretti, J. C. G. Lavocat, C. H. Ho, C. Parmeggiani, and D. S. Wiersma, "High-resolution 3D direct laser writing for liquid-crystalline elastomer microstructures," Adv. Mater. **26**(15), 2319–2322 (2014).
113. H. Zeng, P. Wasylczyk, C. Parmeggiani, D. Martella, M. Burresi, and D. S. Wiersma, "Light-fueled microscopic walkers," Adv. Mater. **27**(26), 3883–3887 (2015).
114. D. Martella, S. Nocentini, D. Nuzhdin, C. Parmeggiani, and D. S. Wiersma, "Photonic microhand with autonomous action," Adv. Mater. **29**(42), 1704047 (2017).
115. D. Martella, D. Antonioli, S. Nocentini, D. S. Wiersma, G. Galli, M. Laus, and C. Parmeggiani, "Light activated non-reciprocal motion in liquid crystalline networks by designed microactuator architecture," RSC Advances **7**(32), 19940–19947 (2017).
116. E. Descrovi, F. Pirani, V. P. Rajamanickam, S. Licheri, and C. Liberale, "Photo-responsive suspended micro-membranes," J. Mater. Chem. C Mater. Opt. Electron. Devices **6**(39), 10428–10434 (2018).
117. S. Nocentini, D. Martella, C. Parmeggiani, S. Zanotto, and D. S. Wiersma, "Structured optical materials controlled by light," Adv. Opt. Mater. **6**(15), 1800167 (2018).
118. S. Nocentini, F. Riboli, M. Burresi, D. Martella, C. Parmeggiani, and D. S. Wiersma, "Three-dimensional photonic circuits in rigid and soft polymers tunable by light," ACS Photonics **5**(8), 3222–3230 (2018).
119. A. M. Flatae, M. Burresi, H. Zeng, S. Nocentini, S. Wiegele, C. Parmeggiani, H. Kalt, and D. Wiersma, "Optically controlled elastic microcavities," Light Sci. Appl. **4**(4), e282 (2015).
120. S. Nocentini, D. Martella, C. Parmeggiani, and D. S. Wiersma, "Photoresist design for elastomeric light tunable photonic devices," Materials (Basel) **9**(7), 525 (2016).
121. C. P. Jisha, K.-C. Hsu, Y. Lin, J.-H. Lin, C.-C. Jeng, and R.-K. Lee, "Tunable pattern transitions in a liquid-crystal-monomer mixture using two-photon polymerization," Opt. Lett. **37**(23), 4931–4933 (2012).
122. C. C. Tartan, P. S. Salter, T. D. Wilkinson, M. J. Booth, S. M. Morris, and S. J. Elston, "Generation of 3-dimensional polymer structures in liquid crystalline devices using direct laser writing," RSC Advances **7**(1), 507–511 (2017).
123. H. Yoshida, "Functionalisation of cholesteric liquid crystals by direct laser writing," Liq. Cryst. Today **21**(1), 3–19 (2012).
124. C. C. Tartan, P. S. Salter, M. J. Booth, S. M. Morris, and S. J. Elston, "Localised polymer networks in chiral nematic liquid crystals for high speed photonic switching," J. Appl. Phys. **119**(18), 183106 (2016).
125. C. C. Tartan, J. J. Sandford O'Neill, P. S. Salter, J. Aplinc, M. J. Booth, M. Ravnik, S. M. Morris, and S. J. Elston, "Read on demand images in laser-written polymerizable liquid crystal devices," Adv. Opt. Mater. **6**(20), 1800515 (2018).
126. D. Franklin, Y. H. Lee, Z. He, D. Chanda, and S. T. Wu, "Large area multi-layer liquid crystal phase modulators enabled by two-photon polymerization," in SID Int. Symp. Digest Tech. Papers **49**(1), 585–588 (2015).
127. L. Yang, J. Li, Y. Hu, C. Zhang, Z. Lao, W. Huang, and J. Chu, "Projection two-photon polymerization using a spatial light modulator," Opt. Commun. **331**, 82–86 (2014).
128. G. Bautista, M. J. Romero, G. Tapang, and V. R. Daria, "Parallel two-photon photopolymerization of microgear patterns," Opt. Commun. **282**(18), 3746–3750 (2009).
129. K. Obata, J. Koch, U. Hinze, and B. N. Chichkov, "Multi-focus two-photon polymerization technique based on individually controlled phase modulation," Opt. Express **18**(16), 17193–17200 (2010).
130. D. Karalekas and A. Aggelopoulos, "Study of shrinkage strains in a stereolithography cured acrylic photopolymer resin," J. Mater. Process. Technol. **136**(1–3), 146–150 (2003).
131. M. P. Patel, M. Braden, and K. W. M. Davy, "Polymerization shrinkage of methacrylate esters," Biomaterials **8**(1), 53–56 (1987).

132. H. B. Sun, T. Suwa, K. Takada, R. P. Zaccaria, M. S. Kim, K.-S. Lee, and S. Kawata, "Shape precompensation in two-photon laser nanowriting of photonic lattices," Appl. Phys. Lett. **85**(17), 3708–3710 (2004).
133. A. A. Bauhofer, S. Krödel, J. Rys, O. R. Bilal, A. Constantinescu, and C. Daraio, "Harnessing photochemical shrinkage in direct laser writing for shape morphing of polymer sheets," Adv. Mater. **29**(42), 1703024 (2017).